Chapter 2

Thermal equilibrium of the plasma

2.1 Introduction

The purpose of this Chapter is to describe the model we propose for solving the global thermal equilibrium of tokamak plasmas using a precise geometry, composition, and arbitrary profiles for density and temperature. In such a model, the conductive-convective transport losses are described by a global energy confinement time, which is empirically deduced from the analysis of a large dataset of discharges from present-day tokamaks. Different kinds of transitions between confinement regimes are considered, and the helium fraction is calculated self-consistently imposing the ratio of the apparent helium confinement time to the energy confinement time.

Description of stability limits of the plasma (pressure, density, and safety factor), as well as characteristics of the inductive and non-inductive mode of operation, are given.

The model for the global thermal equilibrium is of considerable importance both for providing the design basis of future devices and for predicting their performance.

2.2 The thermal equilibrium equation

In steady-state conditions ($\frac{d}{dt} = 0$) the thermal power sources of the tokamak plasma are balanced by the thermal power losses

$$P_{\alpha} + P_{\mathrm{OH}} + P_{\mathrm{add}} = P_{\mathrm{B}} + P_{\mathrm{syn}} + P_{\mathrm{con}}, \tag{2.1}$$

where P_{α} is the alpha power coupled to the plasma, i.e. the power supplied to the plasma by the alpha particles resulting of the fusion reactions, P_{OH} is the ohmic power source, P_{add} is the additional power source, P_{B} is the Bremsstrahlung radia-

tion loss, P_{syn} is the synchrotron radiation loss, and P_{con} represents the conductive-convective transport losses.

2.2.1 Plasma composition

Burning plasmas considered here are composed of an equal mixture of Deuterium (D) and Tritium (T) ($n_D = n_T$), which produces the most promising fusion reaction, of helium ions (alpha particles) with $Z_{\text{He}} = 2$ as well as of two impurity species with atomic numbers Z_1 and Z_2.

Denoting the electron density as n_e and considering the quasi-neutrality equation ($n_e = \sum n_i Z_i$), the effective atomic number Z_{eff}, which is defined as $Z_{\text{eff}} = \sum f_i Z_i^2$, may be written as

$$Z_{\text{eff}} = 1 + 2f_{\text{He}} + f_1 Z_1 \left(Z_1 - 1\right) + f_2 Z_2 \left(Z_2 - 1\right),$$

where $f_i = n_i/n_e$ is the impurity fraction of the ion species i, e.g.

$$f_{\text{DT}} = 1 - 2f_{\text{He}} - Z_1 f_1 - Z_2 f_2.$$

2.2.2 Plasma power sources

The number of D-T fusion reactions occurring in the plasma volume is

$$N_{\text{fus}} = \int_V n_{\text{D}} n_{\text{T}} \, \overline{\sigma v}_{\text{DT}}(T_i) \, dV,$$

where $\overline{\sigma v}_{\text{DT}}(T_i)$ is the D-T thermonuclear reaction rate for two D and T maxwellian populations (n_{D} and n_{T}, respectively) with the same ion temperature T_i. The expression used for $\overline{\sigma v}_{\text{DT}}(T_i)$ is the Sadler fit [Sad87], which is precise for 0 keV $< T <$ 100 keV.

The product of D and T densities is expressed in a most convenient form as a function of the electron density in the following form:

$$n_{\text{D}} n_{\text{T}} = C_\alpha \frac{n_e^2}{4},$$

where C_α is the dilution coefficient in the alpha power source due to the impurities and helium content. We have

$$C_\alpha = \left(1 - 2f_{\text{He}} - Z_1 f_1 - Z_2 f_2\right)^2. \tag{2.2}$$

Typical values for the reactor plasma parameters considered in Chapter 6 are $C_\alpha \sim 0.40 - 0.50$, which means that for a given electron density (as we will see in Section 2.5, n_e is limited by MHD instabilities) the number of D-T fusion reactions

in the presence of impurities and helium are reduced approximately by half with respect to an ideal "clean" plasma ($Z_{\text{eff}} = 1$). This important effect is called the dilution effect. It can be seen that when the impurity fraction of the ion species i is increased by Δf_i, N_{fus} in relative terms is decreased by

$$\frac{\Delta N_{\text{fus}}}{N_{\text{fus}}} = \frac{Z_i \Delta f_i}{C_{\alpha_0}} \left(Z_i \Delta f_i - 2C_{\alpha_0}^{1/2} \right)$$

with C_{α_0} the initial dilution coefficient. As an example, for $Z_i = 4$ and $C_{\alpha_0} = 0.5$, N_{fus} is reduced by about 11% when $\Delta f_i = 1\%$.

The total fusion power produced inside the plasma may be written as

$$P_{\text{fus}} = N_{\text{fus}} \left(E_\alpha + E_n \right), \tag{2.3}$$

where E_α is the initial kinetic energy of the alpha particle (3.56 MeV)[1] and E_n is the kinetic energy of the neutron (14.0 MeV), but only the alpha particles are thermalized into the plasma. Thus the power that contributes to heat the plasma is the alpha power, which can be expressed as

$$P_\alpha = F_{P_\alpha} N_{\text{fus}} E_\alpha, \tag{2.4}$$

where F_{P_α} is the fraction of the alpha power produced by the fusion reactor which is effectively coupled to the plasma. Typical values of this fraction are $F_{P_c} \sim 95 - 100\%$. In this work, we assume $F_{P_c} = 1$.

Fig. 2.1 shows the maximum fusion power ever produced in JET and TFTR devices.

The toroidal current which is necessary for the magnetic equilibrium in a tokamak is also a source of plasma heating due to the resistivity originating in electron-ion collisions. The ohmic heating power in the plasma balance is given by

$$P_{\text{OH}} = \int_V \eta j_{\text{OH}}^2 dV$$

where η is the plasma resistivity and j_{OH} is the ohmic current density, which is driven by the toroidal electric field induced by the variation of the magnetic flux in the poloidal system of the tokamak (transformer action). Note that from a point of view of the thermal energy plasma balance, the self-generated current I_{BS} (also called bootstrap current) and the externally driven current I_{CD} (generated by the current drive methods) do not participate to the ohmic power source,

$$I_{\text{OH}} = \int_S j_{\text{OH}} dS = I_p - I_{\text{BS}} - I_{\text{CD}},$$

[1] Here the kinetic energy of the thermalized He ion is neglected in comparison with the initial alpha particle energy.

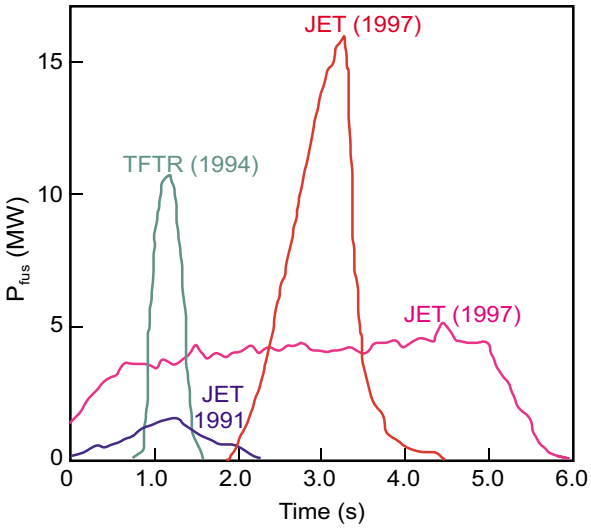

Figure 2.1: Thermonuclear power generation versus time (arbitrary zero). Source: Ref. [Wat99].

where I_p is the total plasma current and S is the plasma poloidal surface.

Hence, in a non-inductive operation, where the toroidal electric field is zero, the ohmic power vanishes.

A neo-classical enhancement factor γ_{NC} is added to the full Spitzer expression for the local plasma resistivity η [Wes97], leading to

$$\eta = \frac{\eta_0 \, Z_{\text{eff}} \ln\Lambda}{T_e^{3/2}} \gamma_{\text{NC}}(A, \rho),$$

with

$$\eta_0 = 0.51 \frac{m_e^{1/2} e^2}{3\varepsilon_0^2 \, (2\pi)^{3/2}} \simeq 1.66 \times 10^{-9},$$

$$\gamma_{\text{NC}}(A, \rho) = \frac{1}{1 - \frac{1.95}{A^{1/2}} \rho^{1/2} + \frac{0.95}{A} \rho},$$

where T_e is the electron temperature, A is the aspect ratio ($A = R/a$) and ρ is the normalized radius (i.e. the polar co-ordinate in the poloidal cross-section normalized to the minor radius a).

The Coulomb logarithm $\ln\Lambda$ may be expressed as $\ln\Lambda = \lambda_D / r_0$, where λ_D is the Debye length ($\lambda_D = \sqrt{\frac{\varepsilon_0 k T_e}{e^2 n}}$) and r_0 is the impact parameter for a 90° scattering, which from a temperature higher than 36 eV is the quantum mechanical length ($r_0 =$

$\frac{\hbar}{2\sqrt{3m_e kT_e}}$). Thus

$$\ln\Lambda = \frac{2\sqrt{3}m_e^{1/2}\varepsilon_0^{1/2}k}{e\hbar}\frac{T_e}{n_e^{1/2}}.$$

In steady state, the spatial distribution of the ohmic current density is derived from the equilibrium of a cylindrical plasma, which gives a flat toroidal electric field E (after a time much larger than the skin penetration time),

$$E = \frac{I_{\mathrm{OH}}}{\int_S \frac{1}{\eta} dS} \tag{2.5}$$

leading to the following expressions:

$$j_{\mathrm{OH}}(\rho) = \frac{I_{\mathrm{OH}}}{\eta_0 Z_{\mathrm{eff}} \int_S \frac{1}{\eta} dS} \frac{T_e(\rho)^{3/2}}{\ln\Lambda(\rho)\ \gamma_{\mathrm{NC}}(\rho)}$$

and

$$P_{\mathrm{OH}} = \frac{\eta_0\, Z_{\mathrm{eff}}\, I_{\mathrm{OH}}^2}{\left(\int_S \frac{T_e(\rho)^{3/2}}{\ln\Lambda(\rho)\,\gamma_{\mathrm{NC}}(\rho)} dS\right)^2} \int_V \frac{T_e(\rho)^{3/2}}{\ln\Lambda(\rho)\,\gamma_{\mathrm{NC}}(\rho)} dV.$$

At high temperatures, the ohmic heating is strongly decreased, as $\eta \propto T_e^{-3/2}$, and for next step scenarios it can be shown that $P_{\mathrm{OH}} \ll P_\alpha$; e.g., the reference scenario in inductive operation for ITER-FEAT predicts $P_{\mathrm{OH}} \simeq 1$ MW to be compared to $P_\alpha \simeq 83$ MW.

The additional power source P_{add} is the global heating power externally injected into the plasma. It includes neutral beam injection heating as well as high frequency wave heating, i.e. ion cyclotron resonance heating, lower hybrid resonance heating, and electron cyclotron resonance heating.

A measure of the success in approaching reactor conditions is given by the amplification factor Q, also called plasma gain, defined as the ratio of the thermonuclear power P_{fus} produced by the plasma (Eq. (2.3)) to the total external power $P_{\mathrm{ext}} = P_{\mathrm{OH}} + P_{\mathrm{add}}$ injected into the plasma,

$$Q = \frac{P_{\mathrm{fus}}}{P_{\mathrm{ext}}} = \frac{1}{F_{P_\alpha}} \frac{E_\alpha + E_n}{E_\alpha} \frac{P_\alpha}{P_{\mathrm{ext}}}.$$

Note that for burning plasmas (like next step or reactor plasmas) the temperature is high enough to have an ohmic heating much lower than the fusion power. In such cases, the external power is approximately equal to the additional heating power. Characteristic values of the amplification factor are $Q = 1, 5, 10, \infty$. $Q = 1$ is called the break-even condition because in this case the fusion power produced is exactly equal to the external power coupled to the plasma. Considering the fact that

$$C_5 = \frac{1}{F_{P_\alpha}} \frac{E_\alpha + E_n}{E_\alpha} \approx 5, \tag{2.6}$$

$Q = 5$ corresponds to an alpha heating power which is roughly equal to the external heating power, $Q = 10$ corresponds to an alpha heating power which is roughly double the external heating power, and $Q = \infty$ is called ignition. In this latter case, the plasma is self-sustained (no external power required).

2.2.3 Plasma power losses

In a magnetic confinement system there is a loss of energy from the plasma by means of different physical mechanisms of transport: radiation losses (P_{rad}) and conduction-convection losses (P_{con}).

Radiation losses:

The plasma core emits electromagnetic radiation due to the acceleration of the charged particles. Electrons are subject to much larger acceleration than ions because of their lighter mass. Therefore, they radiate much more strongly and only the electrons need to be considered here.

Depending on the origin of the acceleration of the electrons, the core radiation losses can be divided in Bremsstrahlung and synchrotron radiation. Bremsstrahlung radiation is emitted in the range of the X-rays wavelengths mainly due to the electron-ion collisions. In the non-relativistic Born approximation, the Bremsstrahlung loss is given by

$$P_{\text{B}} = \int_V C_{\text{B}}\, Z_{\text{eff}}\, n_e^2 T_e^{1/2}\, dV, \tag{2.7}$$

with

$$C_{\text{B}} = \frac{1}{(4\pi\epsilon_0)^3} \frac{32\sqrt{2}}{3\sqrt{\pi}} \frac{e^6 k^{1/2}}{m_e^{3/2} c^3 \hbar} \simeq 5.355 \times 10^{-37},$$

The dependence of P_{B} in Z_{eff} together with the dilution effect introduced previously, makes low impurity content essential for thermonuclear plasmas. As an example, for $Z_i = 4$ and $Z_{\text{eff}} = 1.9$, P_{B} is increased by about 6% when $\Delta f_i = 1\%$. Comparing both impurity effects on the thermal energy balance of commercial reactor plasmas, the dilution effect is the dominant one since in such conditions the alpha power coupled to the plasma is much higher than Bremsstrahlung losses.

Synchrotron radiation has its origin in the gyromotion of the electrons around the magnetic field lines confining the plasma. Owing to the complexity of their exact calculation, synchrotron radiation losses per unit of plasma volume are roughly estimated by expressions deduced for homogeneous cylindrical plasmas, of the form [Tru79]

$$P_{\text{syn}} \simeq 8.2 \times 10^{-10}\, (1 - r)^{1/2}\, R a^{3/2} T_e^{5/2} B_{t_0}^{5/2} n_e^{1/2},$$

where R and a are the major and minor radius of the tokamak, B_{t_0} is the magnetic field on the plasma axis, and r is the reflection coefficient of the machine first wall.

The emission is in the millimetre wavelength region. Consequently, the emitted radiation is both absorbed by the plasma itself and reflected by the first wall, resulting in a new absorption phase so that the power effectively lost is negligible compared to the power balance, for plasmas of present tokamaks. However, in Chapter 6 we illustrate that synchrotron losses become significant in the power balance of high-temperature plasmas envisaged for a steady state commercial reactor. The complete formalism for the synchrotron radiation transport will be described in Chapter 3, where a new expression for the fast calculation of synchrotron losses is proposed.

The presence of impurities in the plasma produces an enhancement of radiation losses. On the one hand, the Bremsstrahlung radiation increases because of the higher value of the effective charge of the plasma. On the other hand, several atomic physics processes such as ionisation by electron collisions, radiative recombination, charge exchange recombination and excitation produce the so-called line radiation. The reaction rates of all of these processes depend on the local plasma electron temperature and on the impurities atomic number. Considering that heavy impurities (metals) and the associated line radiation in a thermonuclear plasma core must be absolutely avoided, the line radiation is maximal at low temperatures, i.e. of the order of tens of eV for the low Z impurities and of the order of 1 keV for medium Z impurities, and it vanishes for core temperatures in which such species are fully ionised. Therefore, line radiation losses are only important at the plasma edge, where they participate in dissipating the conductive-convective heat flux, not affecting the global power balance.

A good estimation of the power that a plasma can radiate by these processes occurring at the plasma mantle (edge plasma inside the separatrix) is provided by the experimental multi-machine expression [Mat97]:

$$P_{\text{rad-mantle}} = \frac{10^{-33}}{5.6} \left(\overline{n_e}\right)^{1.95} S^{1.03} \frac{Z^*_{\text{eff}} - 1}{Z_r^{0.19}}, \tag{2.8}$$

where

$$Z^*_{\text{eff}} = 1 + f_r Z_r \left(Z_r - 1\right),$$

S is the plasma surface, and f_r and Z_r are the fraction and atomic number of the radiative impurity (Neon or Argon in next step tokamaks). In the plasmas with two impurity species considered in this work, we take $f_r = f_2$ and $Z_r = Z_2$. The above expression is obtained from that in Ref. [Mat97] by replacing $Z_{\text{eff}} - 1$ by $Z^*_{\text{eff}} - 1$ only taking into account the contribution to Z_{eff} of the radiative impurity $f_r Z_r \left(Z_r - 1\right)$, which corresponds to the case where the temperature pedestal is high enough so that light impurities no longer radiate.

Conductive-convective loss and energy confinement time:

The conduction-convection loss P_{con} is the power transferred from the core to the edge plasma by conduction and convection processes. It is modelled through the global energy confinement time τ_E by the following expression:

$$P_{\text{con}}\left(n_e, T_e\right) = \frac{W_{\text{th}}\left(n_e, T_e\right)}{\tau_E\left(n_e, P_{\text{net}}\right)}, \tag{2.9}$$

where W_{th} is the total energy content of the plasma and P_{net} is the so-called net heating power, i.e. the power coupled to the plasma which is not lost by the core radiation processes. The expression of P_{net} is as follows:

$$P_{\text{net}} = P_{\text{tot}} - \left(P_{\text{B}} + P_{\text{syn}}\right)$$

with

$$P_{\text{tot}} = P_{\alpha} + P_{\text{OH}} + P_{\text{add}},$$

which means that at thermal equilibrium, we have

$$P_{\text{net}} = P_{\text{con}}. \tag{2.10}$$

Considering a multispecies plasma with a temperature T_e for the electrons and T_i for the ions and impurity species, the thermal energy content in Eq. (2.9) may be written as

$$W_{\text{th}} = \int_V C_W \, 3 n_e k T_e \, dV, \tag{2.11}$$

where C_W is the multispecies coefficient, given by

$$C_W = \frac{1}{2}(1+\theta_i) - \frac{\theta_i}{2}\left[f_{\text{He}} + f_1\left(Z_1 - 1\right) + f_2\left(Z_2 - 1\right)\right] \tag{2.12}$$

with $\theta_i = T_i/T_e$.

2.2.4 Peak heat flux on the divertor target plates

In a reactor plasma, the impurities which come from solid surfaces or resulting from the fusion process (alpha particles) must be controlled to keep an acceptable value of Q, due to the dilution effect and radiation processes. Impurities can also lead to disruptions as a result of edge cooling and consequent current profile modification.

Two techniques are presently used to separate the plasma from the vacuum vessel and to pump out the impurities. The first one, is to define an outer boundary of the plasma with a material limiter as shown in Fig. 2.2(a). The second technique is

to keep the particles away from the vacuum vessel by means of a modification of the magnetic field so that, outside the last closed magnetic surface (LCMS), the plasma flows towards and eventually interacts with a solid surface. This is the basic geometry of a divertor (see Fig. 2.2(b)). The essential difference between the two methods is that with a limiter the LCMS is in contact with a solid surface, whilst with a divertor the solid surface may be placed at some distance from the LCMS. For next step devices and reactors the divertor configuration is envisaged.

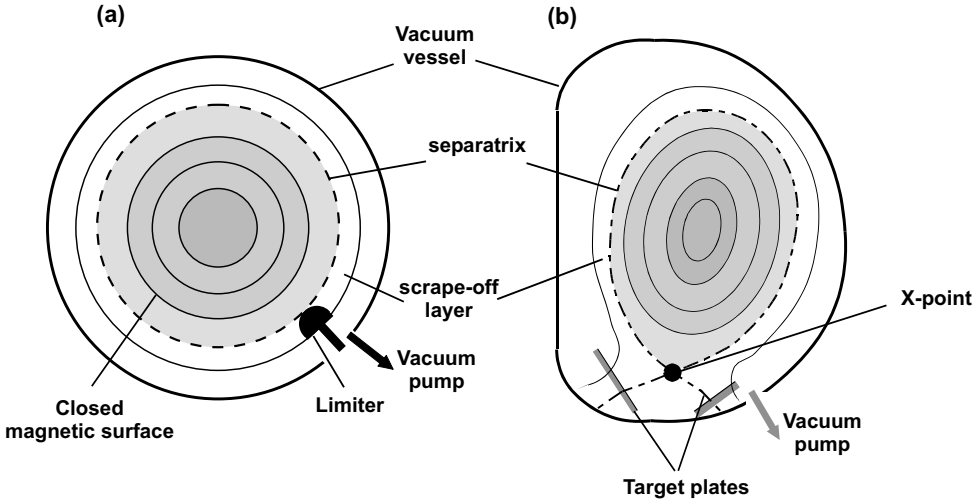

Figure 2.2: Schematic diagram of poloidal flux surfaces in a tokamak (a) with a limiter configuration and (b) with a divertor configuration (the toroidal field is normal to the page).

There are several possible magnetic configurations for divertors, but the most successful one has been the toroidal symmetric configuration. The required magnetic field is produced by creating a null in the poloidal field, separating closed and open magnetic surfaces (X-point). It has been found experimentally that the use of such a divertor configuration also often results in a significant improvement in the energy confinement time, the plasma being in a confinement regime known as the H-mode (see Section 2.4.2). In the present study we only refer to such divertor configurations.

A difficult problem associated with the divertor is that of limiting the power density flowing to the target surface. This is necessary to avoid high surface temperatures which can lead to surface melting, catastrophic impurity release by evaporation or other processes. The time averaged peak heat flux on the divertor target plates is taken to be

$$\Phi_{\text{div-peak}} = 0.62\frac{P_{\text{sep}}}{R}, \tag{2.13}$$

where P_{sep} is the power crossing the separatrix (last closed magnetic surface) and the constant is adjusted to obtain $\Phi_{\text{div-peak}} = 10$ MW/m^2 for $P_{\text{sep}} = 100$ MW in ITER-FEAT ($R = 6.2$ m). The $1/R$ dependence is due to the fact that the width of the scrape-off layer is approximately kept constant with increasing machine dimensions.

2.3 Conductive-convective heat transport within a fusion plasma

2.3.1 Determination of the global energy confinement time τ_E from a local modelling of heat transport

In a magnetic plasma configuration, the confinement properties are governed by the transport perpendicular to the magnetic field, since the parallel transport is much larger than the perpendicular one. Hence, axisymmetry is considered in the plasma torus and consequently the density and the temperature are constant on a magnetic surface, which complies with the equilibrium condition

$$\mathbf{j} \times \mathbf{B} = \boldsymbol{\nabla} p,$$

where $\mathbf{j} \times \mathbf{B}$ is the magnetic force ($\mathbf{j}$ the current density flux and $\mathbf{B}$ the magnetic field) and $\boldsymbol{\nabla} p$ is the force due to the plasma pressure.

For a given magnetic surface, the differential formulation of the conservation equation for the thermal energy w_{th} per unit of volume can be written as

$$\frac{d}{dt} w_{\text{th}} + \boldsymbol{\nabla} \cdot \boldsymbol{\phi} = p_{\text{net}}, \tag{2.14}$$

where p_{net} is the net heating power per unit of volume corresponding to the magnetic surface, and $\boldsymbol{\phi}$ is the heat flux across the magnetic surface. In steady-state ($\frac{d}{dt} w_{\text{th}} = 0$), Eq. 2.14 leads to

$$\boldsymbol{\nabla} \cdot \boldsymbol{\phi} = p_{\text{net}}. \tag{2.15}$$

In the first approximation, the conductive heat flux $\boldsymbol{\phi}_j$ for each species in a thermonuclear plasma can be locally expressed in terms of density n_j and temperature T_j by the differential Fourier form

$$\boldsymbol{\phi}_j = -n_j k \chi_j \boldsymbol{\nabla} T_j, \tag{2.16}$$

where χ_j is the thermal diffusivity of the species j. The units of χ_j are $\left[\frac{m^2}{s}\right]$ for a heat flux $\boldsymbol{\phi}$ expressed in $\left[\frac{J}{m^2 s}\right]$.

The problem of the local modelling of heat transport can be reduced to the estimation of the thermal diffusivity coefficient χ_j. Then, for a given χ_j model, the

temperature profiles may be deduced from Eqs (2.15) and (2.16) when the profile of density and source of heating power p_{net} are known.

In thermal equilibrium, integration of the transport equations (2.15) and (2.16) then leads to the zero D equilibrium equation (2.1) with P_{con} given by Eq. (2.9). Note that the convective part of transport could be added to the conductive term ϕ_j for each species, keeping the validity of the zero D power equilibrium when transport equations are integrated.

2.3.2 Classical, neoclassical and anomalous models for the thermal diffusivity

In the absence of instabilities the confinement is determined by Coulomb collisions. The transport of energy and particles which would occur in these circumstances has been calculated. Nevertheless, the predicted results cannot explain the experimental results even though the neoclassical effects are considered. In particular, the experimental thermal transport by electrons and the consequent thermal diffusivity are up to two orders of magnitude higher than neoclassical predictions.

It is thought that the observed anomalous transport is due to micro-instabilities of the plasma. Today, a large international collaborative effort is being done in order to understand and model this so-called anomalous transport using the non-linear kinetic theory. Although the key parameters leading to a growth rate of the instabilities onset are identified [Bou00], today there is no satisfactory agreement between the theory calculations and the experimental behaviour. For this reason, it has been necessary to resort to empirical methods providing statistical scaling expressions deduced from experimental tokamak results which, within some error, allow extrapolation to next step tokamaks.

Classical transport:

In a cylindrical plasma the collisional transport of particles and energy can be understood in terms of a simple diffusion process, and this is called classical transport. Electron and ion thermal diffusivities can be estimated by assuming Coulomb interactions to be produced between identical particles with different thermal energy. Thus,

$$D_e \sim \chi_e,$$

where D_e is the electron diffusivity.

On the other hand, the ion thermal diffusivity is related to the electron thermal diffusivity as a ratio between masses

$$\chi_i \sim \left(\frac{m_i}{m_e}\right)^{1/2} \chi_e,$$

with the consequent prediction that the ion thermal diffusivity would far exceed that of the electrons.

In a random walk approach we assume that, due to the collisions with other particles characterized by the collision frequency ν_c, a particle makes a step perpendicular to the magnetic field with a step length equal to the Larmor radius ρ_L, which is the orbit radius described by a particle in the presence of a magnetic field on its perpendicular plane,

$$\rho_L = \frac{m\upsilon_\perp}{eB}.$$

This gives a diffusion coefficent

$$D_e \sim \frac{\Delta x^2}{\Delta t} \sim \rho_L^2 \nu_c.$$

The thermal diffusivities experimentally determined are much larger than the values predicted by the classical transport theory. In addition to this, the electron thermal diffusivity is found to be larger than the ion one. Therefore, classical transport cannot be the dominant process in a fusion plasma.

Neoclassical transport theory:

The magnetic field in a poloidal plasma section is not homogeneous due to the fact that the toroidal coils are closer in the inner part than in the outer part (∇B). In such a distribution of the magnetic field, when a particle's guiding centre follows a curved magnetic field, it undergoes a drift giving rise to two types of guiding centre orbit, as shown in Fig. 2.3.

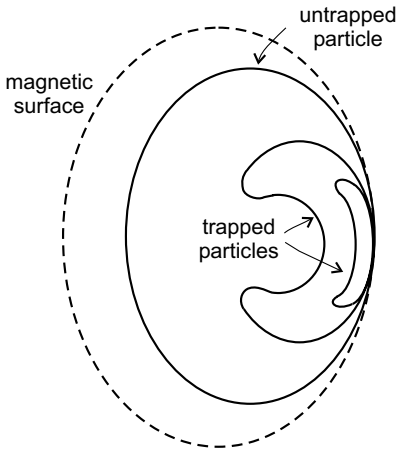

Figure 2.3: Poloidal plane projection of the guiding centre orbit of untrapped and trapped particles. The major axis of the tokamak is on the left.

For magnetic field lines with sufficiently high $v_\perp/v_\parallel$, the particles can be trapped because their parallel velocity $v_\parallel$ is not sufficient to escape the magnetic well which is formed as a result of the poloidal variation of B. The projection of the trapped particles orbit on a poloidal plane has not enclosed the magnetic axis, but rather has a banana-like shape due to the curvature drift. A simple result of this effect is that the electrical conductivity is lowered in neoclassical theory, as trapped particles cannot contribute to the toroidal current.

The existence of banana orbits leads to the so called effective collision frequency for trapped particles $\nu_{\text{eff}} \sim \nu_c/\varepsilon$, where ν_c is the collision frequency between particles and ε is the inverse aspect ratio. Let us define the collisionality parameter as

$$\nu^\star = \frac{\nu_{\text{eff}}}{\nu_b},$$

where $\nu_b \sim v_{\text{th}}\varepsilon^{1/2}/\left(qR\right)$ is the inverse of the time a particle needs to transit the banana, v_{th} is the electron thermal velocity, and q is the safety factor (see Section 2.5.3). The normalized collision frequency ν^* determines whether the particle can complete a banana orbit between two collisions. Depending on its value, we define three different regimes, which are illustrated in Fig. 2.4:

- Banana regime (low collision frequency $\nu^\star < \varepsilon^{3/2}$): the effective frequency ν_{eff} of the Coulomb collisions which are able to detrap the trapped particles is lower than the transit frequency in the banana orbit. Thus, the trapped particles follow the banana orbit several times before they are scattered. In this case, the relevant transport mechanism is the diffusion of the trapped particles

  $$D_e \sim \Delta_b^2 \nu_{\text{eff}},$$

  where $\Delta_b \sim q\rho_L\varepsilon^{-1/2}$ is the width of the banana orbit. The effective diffusion coefficient for the banana regime takes into account that only a fraction $\sim \varepsilon^{1/2}$ of the particles are trapped, leading to

  $$D_e \sim q^2\rho_L^2\nu_{\text{c}}\,\varepsilon^{-3/2}.$$

  This diffusion coefficient exceed the classical diffusion coefficient by the large factor $q^2\varepsilon^{-3/2}$.

- Pfirsch-Schlüter regime (high collisionality $\nu^\star > 1$): the trapped particles do not complete their banana orbits but are scattered before. In this case, the diffusion of the untrapped particles determines the transport, and it is found

  $$D_e \sim q^2\rho_L^2\nu_c.$$

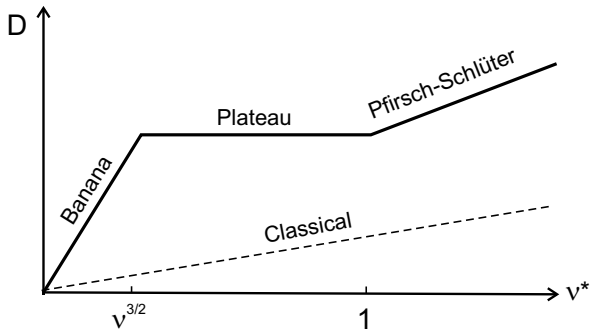

Figure 2.4: Variation of diffusion coefficient with collision frequency throughout the three different transport regimes (solid line), and the predicted classical values (dashed line).

- Plateau regime ($\varepsilon^{3/2} < \nu^{\star} < 1$): between the banana and Pfirsch-Schlüter regimes. In this case, the diffusion coefficient $D_e \sim \upsilon_{\text{th}} \rho_L^2 q/R$ is independent of the collision frequency ν_c.

These neoclassical terms have to be added to the classical terms. In fact, they completely dominate the latter. Nevertheless, the predicted results still cannot explain the experimental observations, especially for electrons.

The anomalous transport:

An approach to the study of the anomalous transport in tokamaks is based on the dimensionless analysis of local scaling expressions for thermal diffusivity. This method provides a reliable way to extrapolate present-day tokamak performance towards a next step device, by maintaining the similarity.

It has been shown that, for a given class of microinstabilities (e.g. electrostatics), the thermal diffusivity depends on a certain local parameters, which are grouped in a dimensionless form. Hence, the thermal diffusivity of each species is usually assumed to scale as [Gar96]

$$\chi \equiv \frac{T}{eB} \left(\rho_L^*\right)^x f\left(\beta, \nu^*\right), \tag{2.17}$$

where ρ_L^* is the Larmor radius normalized to the minor radius a, and $f\left(\beta, \nu^*\right)$ is the dependence on beta and on normalized collision frequency. The so-called gyro-Bohm model is characterized by $x = 1$ in Eq. (2.17), whereas $x = 0$ corresponds to the so-called Bohm model.

At this point, we can make two general considerations. First, we observe that ρ_L^* increases from large to small machines. Secondly, since the normalized Larmor radius depends on the square root of the local temperature of a plasma with a

Maxwellian distribution ($\rho_L^* \propto T^{1/2}$), there is a natural tendency for the gyro-Bohm term to be more important in the plasma centre with respect to the Bohm term, when other functional dependencies are similar.

- The mixed Bohm/gyro-Bohm anomalous transport model

The mixed Bohm/gyro-Bohm model, which is based on such considerations, assumes the transport inside a tokamak plasma to be a combination of a Bohm term that dominates in the plasma edge (χ_{B}), and a gyro-Bohm term that is peaked in the plasma centre and dominates the heat flux in small machines (χ_{gB}). The two terms are added to the neoclassical diffusivity χ_{neo}, giving the following expression for the thermal diffusivity:

$$\chi = \chi_{\mathrm{B}} + \chi_{\mathrm{gB}} + \chi_{\mathrm{neo}}$$

with the following expression for the Bohm-like term χ_{B} for electrons and ions:

$$\chi_{\mathrm{B}e} = \alpha_B \frac{cT_e}{eB_t} \frac{1}{L^*_{p_e}} q^2 \qquad \text{and} \qquad \chi_{\mathrm{B}i} = 2\chi_{\mathrm{B}e},$$

where $L^*_{p_e}$ is the normalized pressure scale length $L^*_{p_e} = \frac{p_e}{a|\nabla p_e|}$, while χ_{gB} is a simple gyro-Bohm-like diffusivity which has the same form for electrons and ions

$$\chi_{\mathrm{gB}} = \alpha_{\mathrm{gB}} \frac{cT_e}{eB_t} \frac{1}{L^*_{T_e}} \rho^*,$$

where $L^{*-1}_{T_e}$ is the normalized temperature scale length $L^*_{T_e} = \frac{T_e}{a|\nabla T_e|}$. The numerical constants α_{B} and α_{gB} are adjusted from the experiments.

The model has been successfully tested on data from different experiments, such as in JET, DIIID, TFTR, ASDEX, and JT-60U, for L-mode confinement regimes[2] [Erb96].

- Extension of the mixed Bohm/gyro-Bohm model to the H-mode regime

In the majority of tokamak plasma configurations, it has been found that when sufficient amount of power is coupled to the plasma, the edge confinement is improved, leading to edge pedestals in the temperature and density. The resulting confinement regime is called the H-mode[3], which is the reference confinement regime for ITER-FEAT. The transport properties in the outer region of the plasma are modified and the numerical value of the diffusivity is reduced by a factor of approximately three. Hence, for H-mode confinement regimes we modify the Bohm term of the thermal diffusivity (dominating the edge transport) by introducing a non-local

[2]The L-mode regime is the "normal" behaviour of a tokamak plasma.

[3]H and L mean "high" and "low" confinement.

dependence on edge parameters. As the diffusivity decreases when the edge temperature is increased (as in the L-H transition), a simple parametric dependence has been proposed [Erb97] by dividing the Bohm diffusivity by the normalized electron temperature scale length $L^*_{T_e}$, evaluated as an average in the boundary region internal to the separatrix corresponding to the normalized toroidal flux co-ordinate $0.8 < \rho < 1.0$, resulting in

$$\chi = \chi_{\mathrm{B}} \left\langle L^*_{T_e} \right\rangle^{-1} + \chi_{\mathrm{gB}} + \chi_{\mathrm{neo}},$$

with

$$\left\langle L^*_{T_e} \right\rangle^{-1} = \frac{T_{e(\rho=0.8)} - T_{e(\rho=1)}}{T_{e(\rho=1)}}.$$

- Extension of the mixed Bohm/gyro-Bohm model to optimized shear configurations

  More recently, new confinement regimes called advanced tokamak regimes have been achieved in several tokamaks [Fuj99], [Wat99], and [All00]. In such regimes, a local stabilising effect (i.e. the local negative magnetic shear) produces a decrease of the instabilities growth rate, creating a so-called internal transport barrier (ITB). The thermal diffusivities inside the ITB are drastically reduced, in some cases even close to neoclassical levels, and the confinement improves. As a result, the density and temperature profiles are steeper in the transport barrier. This strong pressure gradient induces an increase of the rotation shearing rate, which then maintains the confinement high quality. Advanced confinement regimes are very promising as a reactor nominal regime.

  The mixed Bohm/gyro-Bohm model can also describe the central ion and electron temperature rise typical of an internal transport barrier regime if a correction factor F_{shear} reduces the Bohm term, in the region where the rotation shearing rate is larger than a threshold value. Semi-empirical expressions are proposed for this rotation shear threshold in Ref. [Voi98].

2.4 Experimental scaling expressions for the global energy confinement time

As seen above, there is a lack of understanding of the anomalous transport theory and as a result it has been necessary to use semi-empirical local expressions for the thermal plasma diffusivity. For plasma engineering studies, i.e. plasma performance predictions or tokamak design, a zero D model for the thermal equilibrium is used. In this model, the thermal losses are described by the global energy confinement

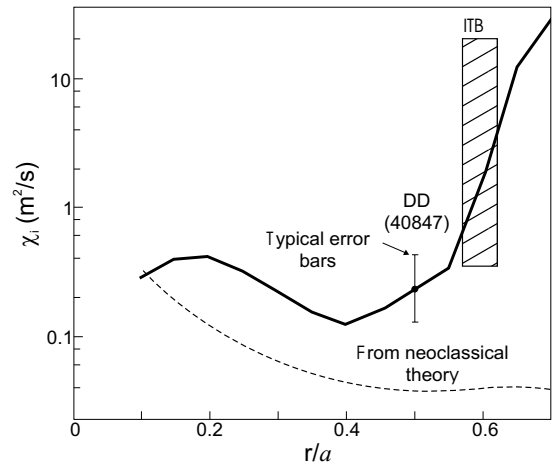

Figure 2.5: Ion thermal diffusivities versus normalized plasma radius for the advanced discharge #40847 of JET, and comparison with neoclassical values [Wat99].

time, which is empirically deduced from the analysis of a large dataset of discharges from present-day tokamaks.

The scaling laws for the global energy confinement time takes a monomial form; that is to say, the product of powers of various engineering plasma parameters. The detailed dependence on these parameters depends on the regimes of plasma confinement, also called modes of confinement.

2.4.1 L-mode

In the L-mode confinement regime, $\tau_E = \tau_{E,\mathrm{L}}$, the ITER-97P(th) expression for the global energy confinement time scaling is considered [FDR97]. We take $\tau_{E,\mathrm{L}} = \tau_{E,\text{ITER-97P(th)}}$, with

$$\tau_{E,\text{ITER-97P(th)}} = 2.3 \times 10^{-10.98} \, \frac{M_{\text{eff}}^{0.2} \kappa_X^{0.64} I_p^{0.96} \left(\overline{n_e}\right)^{0.4} B_{t_0}^{0.03} R^{1.89} a^{-0.06}}{P_{\text{net}}^{0.73}}, \qquad (2.18)$$

where M_{eff} is the effective mass ($M_{\text{eff}} = 2.5$ for a 50% D-T plasma), κ_X is the up-down averaged value of the plasma elongation at the X-point, and $\overline{n}_e$ is the line averaged density.

It is worth noting that the global energy confinement time exhibits degradation with increasing net heating power.

2.4.2 H-mode

The most convenient operation regime for stationary operation in H-mode is called the ELMy H-mode ($\tau_E = \tau_{E,\mathrm{H}}$). This is the reference confinement regime for ITER-FEAT. The reference scaling for the ITER-FEAT design [IPB99] is a conservative scaling (with respect to other scaling laws proposed before) derived using 1310 points of ELMy H-mode discharges from 11 tokamaks. In this case, we take $\tau_{E,\mathrm{H}} = \tau_{E,\mathrm{IPB98(y,2)}}$, with

$$\tau_{E,\mathrm{IPB98(y,2)}} = 5.62 \times 10^{-11.23} \frac{M_{\mathrm{eff}}^{0.19} \kappa_a^{0.78} I_p^{0.93} \left(\overline{n}_e\right)^{0.41} B_{t_0}^{0.15} R^{1.39} a^{0.58}}{P_{\mathrm{net}}^{0.69}}, \qquad (2.19)$$

where the effective plasma elongation κ_a is the ratio of the LCMS poloidal surface S_p (see Section 2.6) to the surface of the circle forming the same minor radius,

$$\kappa_a = \frac{S_p}{\pi a^2}.$$

The root mean square error of this scaling, which is shown in Fig. 2.6, is RMSE $= 14.5\%$ (see Appendix C for the definition of such a goodness fit indicator).

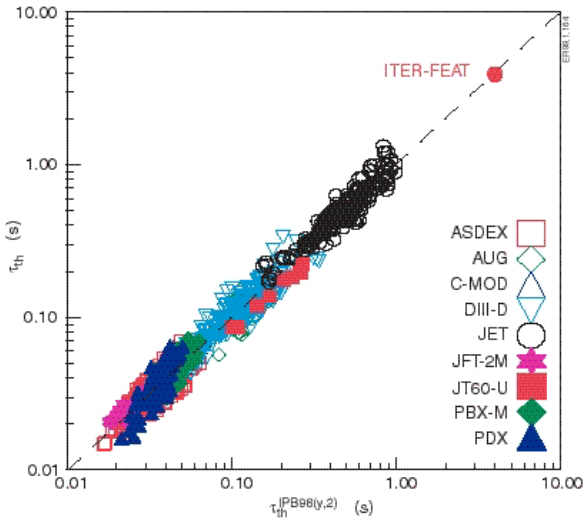

Figure 2.6: Comparison of the experimental energy confinement time τ_{th} with the scaling expression in Eq. (2.19), for ELMy H-mode discharges, and prediction for ITER-FEAT next step (Ref. [ODR99]).

Advanced regimes achieve global confinement times larger than the values predicted by the above scaling. In order to evaluate this improved confinement, the confinement time enhancement factor H_H is introduced using the following relation:

$$\tau_E = H_{\mathrm{H}} \times \tau_{E,\mathrm{IPB98(y,2)}}. \qquad (2.20)$$

Recent near steady-state discharges from JT-60U with ITB have achieved $H_{\rm H} \sim 2.2$ [Kam00]. Other high values of confinement time enhancement factor have been observed on DIII-D [All00] and JET [Wat99].

2.4.3 L-H transition power threshold

Denoting $P_{\rm sep}$ the power crossing the Last Closed Magnetic Surface (LCMS), we have the following relation

$$P_{\rm con} = P_{\rm rad\text{-}mantle} + P_{\rm sep}, \tag{2.21}$$

where $P_{\rm rad\text{-}mantle}$ is the power radiated at the plasma edge inside the separatrix (plasma mantle). When $P_{\rm sep}$ exceeds a threshold value $P_{\rm L\text{-}H}$, the L-H transition occurs, $P_{\rm sep} \geq P_{\rm L\text{-}H}$.

The expression considered for the L-H transition power threshold is that used for the ITER-FEAT design, which is deduced from the analysis of discharges of present-day tokamaks [IPB99],

$$P_{\rm L\text{-}H} = 2.84 \times 10^{-5.6} \left(\overline{n_e}\right)^{0.58} B_{t_0}^{0.82} R^{1.00} a^{0.81} M_{\rm eff}^{-1}. \tag{2.22}$$

In several devices, a power hysteresis has been observed for the H-mode threshold and about $1.5 - 2$ times more power is required to achieve the H-mode (L-H transition) than to sustain it (H-L transition). However, on JET and in high-density discharges on ASDEX-Upgrade, hysteresis is not observed [IPB99]. Thus, as a conservative criterion, for prospective studies (see Chapters 4, 5, and 6) we use the L-H power threshold expression (2.22) also for the H-L transition (no hysteresis).

2.4.4 The L-mode and ELMy H-mode softly mixed scaling $\tau_{E,mix}$

Some experiments have shown a degradation of the H-mode confinement for $P_{\rm sep}$ above the L-H transition power threshold [Jac98] (up to twice the $P_{\rm sep}$ value). In order to model this effect, we introduce a soft transition between the H-mode and L-mode regimes using the following expression:

$$\tau_{E,\rm mix} = \tau_{E,\rm L} + H_\tau^* \left(\tau_{E,\rm H} - \tau_{E,\rm L}\right) \tag{2.23}$$

with

$$\begin{cases} H_\tau^* = 0 & \text{for} \quad P_{\rm sep}/P_{\rm L\text{-}H} \leq 1 \\ H_\tau^* = \left[1 - \left(P_{\rm sep}/P_{\rm L\text{-}H} - 2\right)^2\right]^{1/2} & \text{for} \quad 1 < P_{\rm sep}/P_{\rm L\text{-}H} < 2 \\ H_\tau^* = 1 & \text{for} \quad P_{\rm sep}/P_{\rm L\text{-}H} \geq 2 \end{cases}$$

where $P_{\rm sep}$ is the power crossing the LCMS, and $\tau_{E,\rm L}$, $\tau_{E,\rm H}$ are the empirical scalings introduced above. Fig. 2.7 plots the function H_τ^* versus the quantity $P_{\rm sep}/P_{\rm L\text{-}H}$.

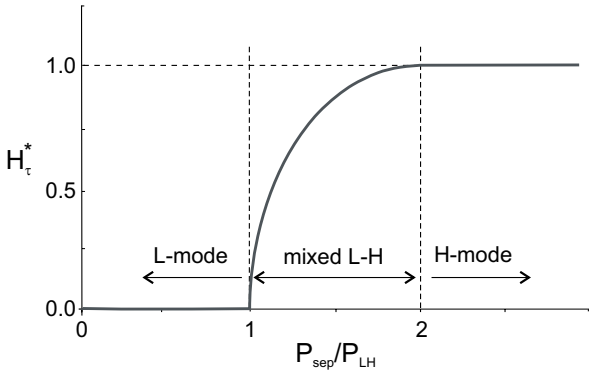

Figure 2.7: Function H_τ^* of the softly mixed scaling between L-mode and H-mode confinement regimes.

When $P_{\text{sep}}/P_{\text{L-H}} \geq 2$ the plasma confinement regime is the H-mode, whilst $P_{\text{sep}}/P_{\text{L-H}} \leq 1$ corresponds to the L-mode regime. Between both cases we have a mixed L-H regime. In Chapter 4, we analyse the plasma performance of ITER-FEAT next step tokamak in this regime.

2.5 Plasma stability domain

The plasma operation window both in inductive or current drive operation is limited by macroscopic magnetohydrodynamical (MHD) instabilities. The constraints for stable plasma operation are on the plasma density, pressure and safety factor.

These constraints are used in prospective and design studies of Chapters 4, 5, and 6.

2.5.1 Density limit

When the electron density reaches a limiting value, unstable plasma processes appear in which a confinement degradation and, in some cases, a disruption (i.e. a dramatic event in which the plasma confinement is suddenly destroyed) are produced. The following empirical expression has been proposed by Greenwald [Gre88] for this density limit:

$$\overline{n}_{\text{Greenwald}} = 10^{14} \frac{I_p}{\pi a^2}, \tag{2.24}$$

where units are SI.

2.5.2 Beta limit

The confined plasma is subject to MHD instabilities which limit the plasma pressure. Let us define the volume averaged toroidal beta $\langle\beta_t\rangle$ measuring the confined pressure as the kinetic pressure due to thermal particles over the toroidal magnetic pressure,

$$\langle\beta_t\rangle = \frac{P_{\text{kinetic}}}{P_{\text{toroidal}}} = \frac{2kC_W \int_V n_e T_e \, dV}{B_{t_0}^2/2\mu_0}, \tag{2.25}$$

where C_W is the multispecies coefficient. We consider the usual normalization of the toroidal beta parameter which is called the normalized beta

$$\beta_{\text{N}} = 10^8 \langle\beta_t\rangle \frac{aB_{t_0}}{I_p}. \tag{2.26}$$

Experiments have been found to be limited to a maximum normalized beta parameter $\beta_{\text{N}\max}$. Typical values are in the range $\beta_{\text{N}\max} \sim 2.5 - 3.0$.

2.5.3 Safety factor

The safety factor q plays an important role in the magnetohydrodynamic stability of the plasma. In general terms, higher values of q lead to greater stability. As seen before, it also appears as a parameter in energy transport theory.

In an axisymmetric configuration, a value of q may be associated to each magnetic surface, which can be defined by

$$q = \frac{\Delta\Psi}{2\pi}, \tag{2.27}$$

where $\Delta\Psi$ is the change of toroidal angle when the field line of a given magnetic surface does a complete poloidal turn. Using the equation of the field line, it is shown that

$$\frac{Rd\Psi}{dl} = \frac{B_t}{B_p}, \tag{2.28}$$

where dl is the distance in the poloidal direction while moving through a toroidal angle $d\phi$, and B_t and B_p are the toroidal and poloidal magnetic fields. Thus, from Eqs (2.27) and (2.28) we obtain

$$q = \frac{1}{2\pi} \oint \frac{1}{R} \frac{B_t}{B_p} dl.$$

For stability analysis, the safety factor is evaluated at the magnetic surface where the poloidal flux is 95% of the total poloidal flux at the separatrix, $q_{\psi 95}$. Applying

Ampere's law in a poloidal plasma section, the averaged poloidal magnetic field at a magnetic surface enveloping the 95% of the plasma may be expressed as

$$\langle B_p \rangle = \mu_0 \frac{I_p}{\oint dl}.$$

In a cylindrical plasma, the expression for the safety factor at the 95% magnetic flux surface is given by

$$q^*_{\psi 95} = \frac{1}{2\pi R} \frac{B_t}{\mu_0 I_p} \left(\oint dl \right)^2,$$

where $\left(\oint dl\right)^2$ is approximated by $(1+K^2)/2$, with $K^2 = \kappa_{95}^2 \left(1 + 2\delta_{95}^2 - 1.2\delta_{95}^3\right)$ and κ_{95} and δ_{95} are the elongation and triangularity of the cross section of the 95% magnetic flux surface.

In the case of toroidal plasmas, the following fit for the safety factor at the 95% magnetic flux surface $q_{\psi 95}$ is used:

$$q_{\psi 95} = \frac{2\pi}{\mu_0} \frac{a^2 B_{t_0}}{R I_p} \frac{1+K^2}{2} \frac{C_{q_1} - C_{q_2}/A}{(1-1/A^2)^2}. \tag{2.29}$$

For limiter plasmas, with no X-points, we will take $\kappa_{95} = \kappa_X = \kappa$, $\delta_{95} = \delta_X = \delta$ and we will use $C_{q_1} = 1.22$, $C_{q_2} = 0.68$. In the case of a configuration with one or two X-points, $q_{\psi 95}$ is given by the above expression with $C_{q_1} = 1.17$, $C_{q_2} = 0.65$.

The minimum safety factor value to guarantee the confinement stability is currently taken to be

$$q_{\Psi 95,\text{min}} \sim 3.$$

2.6 Plasma geometrical description

The tokamak plasma is axysimmetric with respect to the vertical axis of the torus. In the general case, we consider asymmetric magnetic surfaces with respect to the equatorial plane. Hence, the plasma configuration can present two, one, or zero X-points.

The poloidal cross-section of the last closed magnetic surface (LCMS) is enclosed inside a rectangular envelope, as represented in Fig. 2.8. We suppose that the contact points of the vertical sides of this rectangle with the poloidal section are situated on the same horizontal axis. In this case, the LCMS geometry is described by four curves parameterised by the following eight parameters:

$$\kappa_X^{(1)}, \delta_X^{(1)}, \psi^{-(1)}, \psi^{+(1)} \qquad ; \qquad \kappa_X^{(2)}, \delta_X^{(2)}, \psi^{-(2)}, \psi^{+(2)}$$

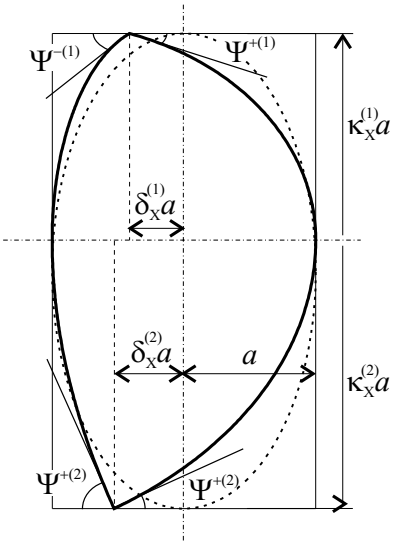

Figure 2.8: General geometry for an asymmetric configuration showing the rectangular envelope and the reference elliptical case.

where κ_X, δ_X are the elongation and triangularity at the X-point, and ψ^-, ψ^+ are the angles between the last closed magnetic surface and the horizontal plane at the internal and external sides of the torus, respectively. The superscripts (1), (2) refer to the upper and lower parts of the poloidal cross-section, respectively.

The curves describing the LCMS are portions of ellipses, parabolas, hyperbolas, or straight lines depending on the values of the geometrical parameters. An example of the LCMS modelling is given in Fig. 2.9. In this case, the upper part of the poloidal section is made of two portions of ellipses as well as the outer lower part. The lower inner part is a portion of hyperbola.

The parametric equations are reported in Appendix A.

2.6.1 Plasma surfaces and volume

For the plasma geometry description presented above, the plasma volume V, and the poloidal and toroidal plasma surfaces (S_p and S, respectively) are calculated using the following explicit expressions:

$$S_p = \pi a^2 \frac{\kappa_X^{(1)} + \kappa_X^{(2)}}{2} \Theta_{S_p},$$

$$S = 2\pi R \times 2\pi a \mathbf{E}_1 \left(\frac{\kappa_X^{(1)} + \kappa_X^{(2)}}{2} \right) \Theta_S,$$

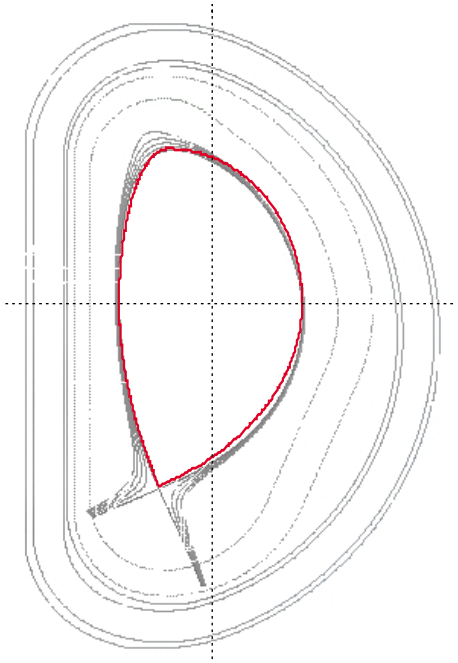

Figure 2.9: Comparison of the poloidal section of the ITER-FEAT Outline Design [ODR99] with our plasma configuration using $\kappa_X^{(1)} = 1.687$, $\kappa_X^{(2)} = 2.001$, $\delta_X^{(1)} = 0.466$, $\delta_X^{(2)} = 0.568$, $\Psi^{-(1)} = 0$, $\Psi^{+(1)} = 0$, $\Psi^{-(2)} = 67.92°$, and $\Psi^{+(2)} = 22.46°$.

$$V = 2\pi R \times \pi a^2 \frac{\kappa_X^{(1)} + \kappa_X^{(2)}}{2} \Theta_V,$$

where Θ_{Sp}, Θ_V, Θ_S are the corrective factors to the pure elliptical cross-section, which is enclosed inside the rectangular envelope (see Fig. 2.8).

Here, a is the plasma horizontal minor radius (half the horizontal side of the rectangular envelope), R is the distance which separates the plasma centre from the vertical axis of the torus, and $\mathbf{E}_1$ is defined as

$$\mathbf{E}_1(\kappa_X) = \frac{2}{\pi} \kappa_X \mathbf{E}\left[(1 - 1/\kappa_X^2)^{1/2}\right],$$

where $\mathbf{E}(k) = E(\frac{\pi}{2}, k)$ is the complete elliptic integral of the second kind. The expressions of the corrections factors as well as of the poloidal surface and volume integrations are deduced in Appendix A.

The plasma configuration defined here allows a very good geometrical description for the configurations of most present tokamak plasmas and next step devices. For example, using the ITER-FEAT parameters and the elevation view of Fig. 2.9, the volume and plasma surfaces calculated with our plasma description differ less than 1% from the values of the ITER-FEAT Outline Design [ODR99].

2.7 Helium content of the plasma

The helium fraction (alpha particles fraction) f_{He} is calculated self-consistently imposing a constant ratio $\tau^*_{\mathrm{He}}/\tau_E$ of the apparent helium particle confinement time to the energy confinement time

$$\tau^*_{\mathrm{He}}/\tau_E = \text{constant},$$

where the apparent helium confinement time τ^*_{He} is the ratio of the total number of He ions present in the discharge to the He source due to fusion reactions.

This condition means that the energy and helium confinement time are linked in a similar way as the thermal and particle diffusivities (see Section 2.3.2). Indeed, recent experiments in the tokamak ASDEX Upgrade have achieved in different discharges identical values for the ratio $\tau^*_{\mathrm{He}}/\tau_E$, in the range of 4 to 6 [ASD98], using a ITER-like divertor configuration (Div II).

By definition, the apparent helium confinement time is the ratio of the total number of He ions present in the discharge N_{He} to the He source due to fusion reactions S_α,

$$\tau^*_{\mathrm{He}} = \frac{N_{\mathrm{He}}}{S_\alpha}.$$

For a volume average electron density $\langle n_e \rangle$,

$$\langle n_e \rangle = \frac{1}{V}\int_V n_e dV \tag{2.30}$$

we obtain

$$\tau^*_{\mathrm{He}} = \frac{f_{\mathrm{He}} E_\alpha \langle n_e \rangle V}{P_\alpha}, \tag{2.31}$$

where P_α is the the alpha power produced inside the plasma.

In order to obtain an unequivocal result of f_{He} in terms of $\tau^*_{\mathrm{He}}/\tau_E$ when the plasma parameters (including density and temperature) are known, we express the energy confinement time τ_E from the monomial scaling laws defined in Section 2.4.

2.7.1 Case of a simple monomial energy confinement time

Considering a thermal equilibrium plasma in which the energy confinement time is described by a scaling law with a power dependence with respect to P_{net}, i.e. the monomial expressions introduced in Section 2.4 as

$$\tau_E = \frac{\tau_E^{(1)}}{P_{\mathrm{net}}^{x_P}}, \tag{2.32}$$

and according to Eqs (2.10) and (2.9), the net heating power follows to be:

$$P_{\text{net}} = \frac{W_{\text{th}}^{\frac{1}{1-x_p}}}{\tau_E^{(1)\frac{1}{1-x_p}}}, \tag{2.33}$$

and the scaling law can be written as

$$\tau_E = \frac{\tau_E^{(1)\frac{1}{1-x_p}}}{W_{\text{th}}^{\frac{x_p}{1-x_p}}},$$

where W_{th} is the thermal content (see Eq. (2.11)), which can be also expressed as $W_{\text{th}} = C_W\left(f_{\text{He}}\right) W_{\text{th}}^{(0)}$, where C_W is the multispecies coefficient given in Eq. (2.12). From Eqs (2.31), (2.32), and (2.33) the ratio of the apparent helium confinement time to the energy confinement time can be written in the form

$$\frac{\tau_{\text{He}}^*}{\tau_E} = \frac{E_\alpha V \left\langle n_e \right\rangle W_{\text{th}}^{(0)\frac{x_p}{1-x_p}}}{P_\alpha^{(0)} \tau_E^{(1)\frac{1}{1-x_p}}} \frac{f_{\text{He}}\left[C_W\left(f_{\text{He}}\right)\right]^{\frac{x_P}{1-x_P}}}{C_\alpha\left(f_{\text{He}}\right)}, \tag{2.34}$$

where $P_\alpha^{(0)}$ is the alpha power defined in Eq. (2.4) of an ideal plasma without impurities nor helium content ($C_\alpha = 1$), thus $P_\alpha = C_\alpha\left(f_{\text{He}}\right) P_\alpha^{(0)}$, while C_α is the dilution coefficient given in Eq. (2.2). In Eq. (2.34) the first term on the right-side depends on the plasma parameters (e.g. density, temperature, magnetic field, plasma current) but not on the helium fraction.

An example of $\tau_{\text{He}}^*/\tau_E\left(f_{\text{He}}\right)$ curve is shown in Fig. 2.10 below showing that this function is monotonic, allowing numerical inversion.

2.7.2 Case of a softly mixed scaling for the energy confinement time

A different treatment must be developed when a softly mixed scaling from the L-mode to the H-mode is considered for the energy confinement time (see Section 2.4.4). In this case, for L-mode and ELMy H-mode scaling laws with a P_{net} dependence as follows

$$\tau_{E,L} = \frac{\tau_{E,\text{L}}^{(1)}}{P_{\text{net}}^{x_{P,\text{L}}}} \qquad \text{and} \qquad \tau_{E,H} = \frac{\tau_{E,\text{H}}^{(1)}}{P_{\text{net}}^{x_{P,\text{H}}}},$$

and according to Eqs (2.31) and (2.9), we obtain the following expressions for the helium fraction in terms of $\tau_{\text{He}}^*/\tau_E$;

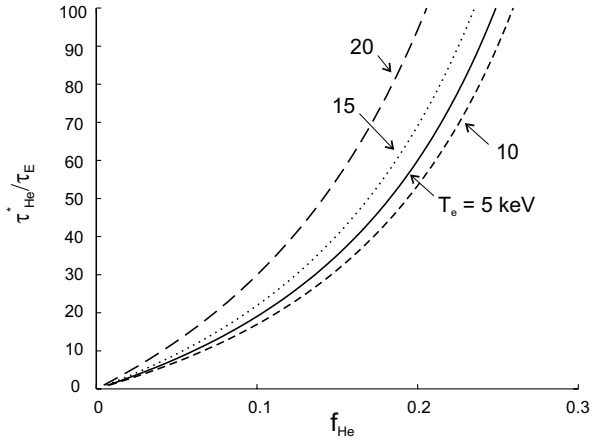

Figure 2.10: $\tau^*_{\mathrm{He}}/\tau_E$ as a function of f_{He} for ITER-FEAT parameters [ODR99], IPB98(y,2) scaling for the energy confinement time, flat density and parabolic temperature profiles, $f_1 = f_2 = 0$, $T_e = T_i$, $\langle n_e \rangle = 10^{20}\mathrm{m}^{-3}$, and $\langle T \rangle = 5, 10, 15, 20$ keV.

for $f_{\mathrm{He}} \leq f_{\mathrm{He,H}}$:

$$(\tau^*_{\mathrm{He}}/\tau_E) = \frac{E_\alpha V \langle n_e \rangle W_{\mathrm{th}}^{(0)\frac{x_{P,\mathrm{H}}}{1-x_{P,\mathrm{H}}}}}{P_\alpha^{(0)} \tau_{E,\mathrm{H}}^{(1)\frac{1}{1-x_{P,\mathrm{H}}}}} \frac{f_{\mathrm{He}} \left[C_W\left(f_{\mathrm{He}}\right)\right]^{\frac{x_{P,\mathrm{H}}}{1-x_{P,\mathrm{H}}}}}{C_\alpha\left(f_{\mathrm{He}}\right)},$$

for $f_{\mathrm{He,H}} < f_{\mathrm{He}} < f_{\mathrm{He,L}}$:

$$C_W\left(f_{\mathrm{He}}\right) W_{\mathrm{th}}^{(0)} = C_{nT}^{1-x_{P,\mathrm{L}}} C_{\alpha 1}^{1-x_{P,\mathrm{L}}} \tau_{E,\mathrm{L}}^{(1)} + \left[1 - \left(C_{nT} C_{\alpha 1} - \frac{P_{\text{rad-mantle}}}{P_{\text{L-H}}} - 1\right)^2\right]^{1/2} \times \left(C_{nT}^{1-x_{P,\mathrm{H}}} C_{\alpha 1}^{1-x_{P,\mathrm{H}}} \tau_{E,\mathrm{H}}^{(1)} - C_{nT}^{1-x_{P,\mathrm{L}}} C_{\alpha 1}^{1-x_{P,\mathrm{L}}} \tau_{E,\mathrm{L}}^{(1)}\right),$$

for $f_{\mathrm{He}} > f_{\mathrm{He,L}}$:

$$(\tau^*_{\mathrm{He}}/\tau_E) = \frac{E_\alpha V \langle n_e \rangle W_{\mathrm{th}}^{(0)\frac{x_{P,L}}{1-x_{P,L}}}}{P_\alpha^{(0)} \tau_{E,\mathrm{L}}^{(1)\frac{1}{1-x_{P,\mathrm{L}}}}} \frac{f_{\mathrm{He}} \left[C_W\left(f_{\mathrm{He}}\right)\right]^{\frac{x_{P,\mathrm{L}}}{1-x_{P,\mathrm{L}}}}}{C_\alpha\left(f_{\mathrm{He}}\right)},$$

with

$$C_{\alpha 1} = \frac{C_\alpha\left(f_{\mathrm{He}}\right) C_W\left(f_{\mathrm{He}}\right)}{f_{\mathrm{He}}} \qquad \text{and} \qquad C_{nT} = \frac{\left(\tau^*_{\mathrm{He}}/\tau_E\right) P_\alpha^{(0)} W_{\mathrm{th}}^{(0)}}{E_\alpha \langle n_e \rangle V},$$

$$f_{\text{He,H}} = \frac{1+\theta_i}{\theta_i} - (Z_1 - 1)\, f_1 - (Z_2 - 1)\, f_2 - \frac{2\tau_{E,\text{H}}^{(1)}\, P_{\text{L-H}}^{1-x_{P,\text{H}}}}{\theta_i W_{\text{th}}^{(0)}} \left(2 + P_{\text{rad-mantle}}/P_{\text{L-H}}\right)^{1-x_{P,\text{H}}},$$

$$f_{\text{He,L}} = \frac{(1+\theta_i)}{\theta_i} - (Z_1 - 1)\, f_1 - (Z_2 - 1)\, f_2 - \frac{2\tau_{E,\text{L}}^{(1)}\, P_{\text{L-H}}^{1-x_{P,\text{L}}}}{\theta_i W_{\text{th}}^{(0)}} \left(1 + P_{\text{rad-mantle}}/P_{\text{L-H}}\right)^{1-x_{P,\text{L}}},$$

while $P_{\text{rad-mantle}}$ and $P_{\text{L-H}}$, which are independent from the helium fraction, are given in Eqs (2.8) and (2.22), respectively. In the first case ($f_{\text{He}} \leq f_{\text{He,H-L}}$) we have a purely H-mode regime, in the third case ($f_{\text{He}} > f_{\text{He,L}}$) we have a purely L-mode regime, and a mixed regime between L-mode and H-mode results from the second case ($f_{\text{He,H}} < f_{\text{He}} < f_{\text{He,L}}$). Therefore, we conclude that, for a given plasma density and temperature, the H-mode regime is maintained whenever the helium fraction is lower than $f_{\text{He,H}}$. Note that when the ratio of the apparent helium confinement time to the energy confinement time is imposed we obtain an unequivocal result for the helium fraction, corresponding to the thermal equilibrium of the plasma.

For all the above cases, the net heating power is simply deduced from the helium fraction as

$$P_{\text{net}} = \frac{(\tau_{\text{He}}^*/\tau_E)\, P_\alpha^{(0)} W_{\text{th}}^{(0)}}{E_\alpha \langle n_e \rangle V} \frac{C_\alpha\left(f_{\text{He}}\right) C_W\left(f_{\text{He}}\right)}{f_{\text{He}}}.$$

Examples of curves of $\tau_{\text{He}}^*/\tau_E$ versus f_{He} and P_{net} curves are shown in Fig. 2.11, showing the existence of only one f_{He} solution for a given $\tau_{\text{He}}^*/\tau_E$.

2.8 Non-inductive current drive operation

In the case of continuous operation of a tokamak with a pure non-inductive current drive method (no loop voltage, no ohmic heating power $P_{\text{OH}} = 0$), the additional power P_{add} is used to drive a current I_{CD} which is the part of the total plasma current I_p which is not due to the bootstrap effect (I_{BS})

$$I_p = I_{\text{CD}} + I_{\text{BS}}.$$

In a reactor based on this principle the poloidal system is simplified and mainly used to maintain the plasma shape and position. Two of the most promising current drive methods are the injection of lower hybrid waves and neutral beam injection [Ane89], experimental evidences of which have been found and studied in present

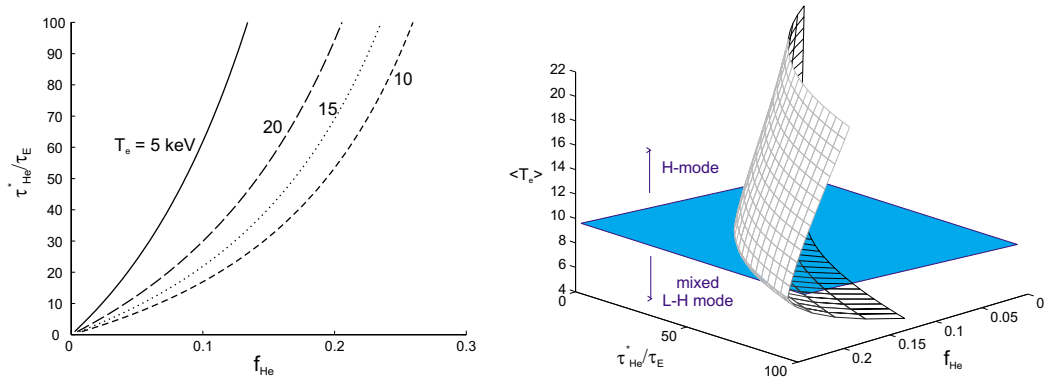

Figure 2.11: $\tau^*_{\mathrm{He}}/\tau_E$ as a function of f_{He} for ITER-FEAT parameters [ODR99], a softly mixed scaling for the energy confinement time, flat density and parabolic temperature profiles, $f_1 = f_2 = 0$, $T_e = T_i = T_\alpha$, $\langle n \rangle = 10^{20}\mathrm{m}^{-3}$, and $\langle T \rangle = 5, 10, 15, 20$ keV. On the right, the plane corresponding to $f_{\mathrm{He},H}$ is shown.

tokamaks [IPB99]. The efficiency γ_{CD} of the current drive method is defined as follows:

$$I_{\mathrm{CD}} = \frac{\gamma_{\mathrm{CD}}}{\langle n_e \rangle R} P_{\mathrm{add}}. \tag{2.35}$$

When the plasma current is driven by different current drive methods at the same time, it may be defined an effective efficiency as

$$\gamma_{\mathrm{CD,eff}} = f^{(\mathrm{CD})}_{\mathrm{NB}} \gamma_{\mathrm{NB}} + f^{(\mathrm{CD})}_{\mathrm{LH}} \gamma_{\mathrm{LH}} + f^{(\mathrm{CD})}_{\mathrm{IC}} \gamma_{\mathrm{IC}} + f^{(\mathrm{CD})}_{\mathrm{EC}} \gamma_{\mathrm{EC}},$$

where $f^{(\mathrm{CD})}_i = P_{\mathrm{CD}i}/P_{\mathrm{add}}$ is the fraction of the total coupled power generated by the i current drive method: neutral beam injection (NB) [Mik83], lower hybrid resonance wave (LH), ion cyclotron resonance wave (IC), and electron cyclotron resonance wave (EC). In this case, $\gamma_{\mathrm{CD,eff}}$ replaces γ_{CD} in Eq. (2.35) and the current drive fraction generated by a given current drive method i is given by

$$I_{\mathrm{CD}i} = I_{\mathrm{CD}} f^{(\mathrm{CD})}_i \frac{\gamma_i}{\gamma_{\mathrm{CD,eff}}},$$

where I_{CD} is the total current drive.

Simulations performed in the framework of ITER studies using any current drive method, show that the efficiency can be simply approximated by [Ton94]:

$$\gamma_{\mathrm{CD}} = \gamma_{0\mathrm{CD}} \langle T_e \rangle \quad \text{with} \quad \gamma_{0\mathrm{CD}} = (0.15 - 0.3) \times 10^{19} \ \mathrm{A\,m^{-2}/(W\,keV)}\,.$$

More precise studies show that $\gamma_{0\mathrm{CD}}$ depends on plasma parameters as Z_{eff}, and density and temperature profiles, but, as a first approach, these effects can be neglected.

2.8.1 Bootstrap current

The bootstrap current is generated by the momentum transfer when trapped particles collide with untrapped ones. In the presence of a density gradient, both trapped ions and electrons carry a parallel current and there is a transfer of momentum to the passing particles of both species, which adjust their velocities accordingly. The difference in velocity between the passing ions and the passing electrons yields the bootstrap current. The bootstrap current is interesting in long pulses or in a continuous tokamak regime, which is requested for a commercial reactor, since it provides part of the tokamak poloidal magnetic field.

The bootstrap current is reduced as the plasma becomes more collisional (ν increases). Thus it is only important in the weakly collisional regimes (banana and plateau) (see Fig. 2.4). An expression of this current is obtained by balancing the momentum exchange between the passing electrons and the passing ions with the momentum exchange between the passing and trapped electrons.

For a circular cross-section tokamak in the large aspect ratio limit (cylindrical plasma) and for a single ion species plasma (ion charge Z_i) with $T_e = T_i$, it can be shown from Ref. [Hin76] that the radial bootstrap current density may be written as:

$$j^*_{\text{BS}}(r) = -\frac{2n_e kT_e}{B_p}\left(\frac{r}{R}\right)^{1/2}\left[\nu(Z_i)\frac{1}{n_e}\frac{dn_e}{dr} + \tau(Z_i)\frac{1}{T_e}\frac{dT_e}{dr}\right]$$

where $\nu(Z_i)$ and $\tau(Z_i)$ are the ion charge coefficients ($\nu = 2.44$ and $\tau = 0.134$ for $Z_i = 1$).

In the case of a toroidal plasma with non-circular cross-section, we use the Wilson fit [Wil92] for the fractional bootstrap current $f_{\text{BS}} = I_{\text{BS}}/I_p$, in which Z_i is replaced by Z_{eff} to take into account several impurity species in the plasma. We have

$$f_{\text{BS}} = \frac{\beta_p}{A^{1/2}} B\left(\alpha_p, \alpha_T, \alpha_j, Z_{\text{eff}}, A\right), \tag{2.36}$$

where α_j, α_T, and $\alpha_p = \alpha_n + \alpha_T$ are the peaking parameters of current density, temperature and pressure, respectively, for profiles described by generalized parabolic expressions (Eq (3.25)). Function B is given in Ref. [Wil92], and β_p is the poloidal beta defined as follows:

$$\beta_p = \frac{2\mu_0 \langle p\rangle}{\langle\langle B_p\rangle\rangle^2} \quad \text{with} \quad \langle\langle B_p\rangle\rangle = \frac{\int B_p d\ell}{\int d\ell}, \quad \text{and} \quad \langle p\rangle = \int_V C_W\, 2n_e kT_e\, dV,$$

where the integration is performed along the poloidal section of the last magnetic surface:

$$\int B_p d\ell = \mu_0 I_p$$

Using

$$\int d\ell = 2\pi a \, \mathbf{E}_1(\kappa_X)\Theta_L \left(\kappa_X, \delta_X, \psi^+, \psi^-\right)$$

we obtain

$$\beta_p = \frac{16\pi^2 k}{\mu_0} \, C_W \, \mathbf{E}_1^2(\kappa_X)\Theta_L^2 \frac{a^2}{I_p^2} \int_V n_e T_e \, dV$$

and

$$f_{\text{BS}} = \frac{16\pi^2 k}{\mu_0} \, C_W \, \mathbf{E}_1^2(\kappa_X)\Theta_L^2 B \, \frac{a^2}{A^{1/2} I_p^2} \int_V n_e T_e \, dV.$$

2.9 Summary

To solve the global thermal equilibrium of tokamak plasmas, plasma power sources and losses are integrated over the plasma volume by considering a precise geometry, composition, and arbitrary profiles for density and temperature. This zero D model considers pure H-mode and L-mode regimes, but also a soft transition between such regimes.

For this plasma geometry description, the calculation of surfaces and plasma volume, as well as the surfaces and volume integrations, are performed by using analytical expressions which have been obtained. The helium fraction is calculated self-consistently imposing a constant ratio of the apparent helium confinement time to the energy confinement time.

The plasma operation window both in inductive and non-inductive operation is limited by MHD instabilities and technological limits such as the peak heat flux on the divertor plates. The constraints for stable plasma operation are on the plasma density, pressure and safety factor.

The plasma model described in this Chapter is used in prospective and design studies of Chapters 4, 5, and 6.